Applied Catalysis B: Environmental 144 (2014) 135–143

Contents lists available at ScienceDirect

Applied Catalysis B: Environmental

journal homepage: www.elsevier.com/locate/apcatb

Promotional effect of transition metal doping on the basicity and activity of calcined hydrotalcite catalysts for glycerol carbonate synthesis

Peng Liu [a,*], Margherita Derchi [b], Emiel J.M. Hensen [a,*]

[a] Department of Chemical Engineering and Chemistry, Eindhoven University of Technology, P.O. Box 513, Eindhoven, The Netherlands
[b] Dipartimento di Ingegneria Chimica, Civile e Ambientale, Università degli Studi di Genova, I-16145 Genova, Italy

ARTICLE INFO

Article history:
Received 11 April 2013
Received in revised form 30 June 2013
Accepted 2 July 2013
Available online 12 July 2013

Keywords:
Heterogeneous catalysis
Transesterification
Hydrotalcite
Reconstruction
Glycerol carbonate

ABSTRACT

A series of transition metal doped hydrotalcites (HT-M) were prepared by using the "memory effect" of hydrotalcites (HT). Further calcination yields mixed oxides with more open structure and tunable basicity. The basicity of the calcined hydrotalcites (HTC-M) strongly depends on the type of transition metal and calcination temperature. The resulting HTC-M materials were used as solid base catalysts and evaluated in the transesterification between glycerol and dimethyl carbonate without using organic solvent. The correlation between the basic properties of the solid catalysts and the catalytic performance was investigated. The activity of HTC-M catalysts was demonstrated to be proportional to the surface density of basic sites. The HTC-Ni calcined at 500 °C exhibited maximum activity, which is about 10 times higher than uncalcined HT precursor for the transesterification reaction. The promotional effect of Ni^{2+} doping could be attributed to the enhancement of the base strength of all three types of basic sites of the calcined hydrotalcite. The HTC-Ni catalyst can be readily recycled while maintaining high catalytic activity and selectivity of glycerol carbonate.

1. Introduction

Heterogeneous base catalysis is an important field of growing interest in both academic and industrial research [1,2]. In practice, the substitution of homogeneous base catalysts (such as metal hydroxides or amines) with solid base catalysts is very attractive in view of the reduction of waste formation, as well as for safety and corrosion aspects [3].

Among various solid bases, hydrotalcite ($Mg_6Al_2(OH)_{16}CO_3{\cdot}nH_2O$) type layered double hydroxides find much industrial interest [4,5] and are the subject of considerable academic investigation [6]. Due to their unique properties such as cation- and anion-exchangeability of the Brucite layer and interlayer, respectively, their tunable surface basicity and the "memory effect" of the layered structure [4,7], hydrotalcite-like compounds have been demonstrated to be effective redox catalysts, solid base catalysts, catalyst precursors and catalyst supports [8]. Being basic in nature hydrotalcites have been widely studied for various base catalyzed or assisted reactions such as alkylation, Michael addition, Claisen–Schmidt condensation, Knoevenagel condensation, aldol condensation, transesterification, hydrogenation, olefin epoxidation and alcohol oxidation [8–15]. Through controlled thermal decomposition, hydrotalcites are converted to mixed oxides with high specific surface areas, homogeneous dispersion of metal cations and strong Lewis basic sites [16,17]. The basic properties of these mixed oxides depend on the composition of metal cations in the precursor hydrotalcite. Interestingly, the catalytic activity of calcined hydrotalcites can also be enhanced by rehydration in an inert atmosphere, which results in reconstruction of the original layered structure, with Brönsted basic sites OH^- as the charge compensating anions in the interlayer [18,19]. Consequently, the facile adjustment of the type of basic sites and surface base strength makes hydrotalcite versatile precursors for optimal solid base catalysts for a wide range of base-catalyzed reactions.

Recently, the utilization of surplus glycerol has received much attention because of the growing biodiesel production [20–22]. Glycerol carbonate (GLC), due to its low toxicity, low flammability, biodegradability and high boiling point, is one of the most important glycerol derivatives and is widely used as protic solvent, chemical intermediate and precursor in the synthesis of polycarbonates, polyurethanes, glycidol-based polymers and surfactants [23,24]. Hydrotalcite-based solid base catalysts have, in particular, shown promise for transformation of glycerol to value-added GLC [25–33]. Zinc-containing hydrotalcite was reported to be effective catalyst for GLC synthesis by carbonylation of glycerol with

* Corresponding authors. Tel.: +31 40 247 2833; fax: +31 40 245 5054.
E-mail addresses: pliu503@hotmail.com, p.liu@tue.nl (P. Liu), e.j.m.hensen@tue.nl (E.J.M. Hensen).

0926-3373/$ – see front matter © 2013 Elsevier B.V. All rights reserved.
http://dx.doi.org/10.1016/j.apcatb.2013.07.010

urea under solvent-free conditions [25]. However, this reaction must be performed at high temperature (>120 °C) and low pressure (30–50 mbar) to shift the equilibrium towards GLC formation by isolating produced ammonia continuously from the gaseous phase, and the catalytic activity is found to be due to the leaching of Zn species into liquid phase thus with a homogeneous reaction nature [26]. A more attractive route for GLC synthesis would be transesterification between glycerol and alkyl carbonates, such as dimethyl carbonate (DMC) and diethyl carbonate (DEC), because of the milder and greener process conditions [23]. Uncalcined MgAl hydrotalcites with co-existent hydromagnesite phase were found to be active catalysts for GLC synthesis from glycerol and DMC [27,28], but a larger amount of catalyst (~50 wt%) and a harmful solvent (*N*,*N*-dimethyl formamide) are needed for this reaction. Medina and co-workers reported that the rehydrated MgAl hydrotalcites showed higher activity than the calcined MgAl mixed oxides for transesterification of DEC with glycerol, but the active reconstructed hydrotalcite catalysts often deactivate rapidly due to the instability of surface Brönsted basic sites [29–31]. Carbon nanofiber supported MgAl hydrotalcites, however, exhibited a different activity trend with calcined mixed oxides showing higher activity than the rehydrated samples, although the calcined catalyst also deactivated upon reuse and showed lower GLC selectivity (<90%) [32]. Zr-doped MgAl hydrotalcite (Mg/Al/Zr = 3/1/1) showed optimal GLC yield when calcined at 650 °C, but without evidence on catalyst stability [33]. Although useful hydrotalcite-based catalysts were reported, it is still a challenging task to develop more efficient and reusable catalysts for synthesis of GLC under mild and solvent-free conditions.

Transition metal-doped hydrotalcites (HT-M) are known to possess tunable surface basic properties that depend on the nature and composition of the transition metal cations [34]. It has been demonstrated that Ni^{2+} or Fe^{3+} containing hydrotalcite-derived mixed oxides are effective solid base catalysts for transesterification in biodiesel production [35–37]. We have recently reported on the benefit of doping transition metal cations into hydrotalcite to render excellent HT-M supported gold nanoparticle catalysts for the aerobic oxidation of alcohols [14]. The basicity of HT-M supports varied with the transition metal (M = Cr^{3+}, Mn^{2+}, Fe^{3+}, Co^{2+}, Ni^{2+}, Cu^{2+}, Zn^{2+}) cations, which potentially enhance the alcohol dehydrogenation activity. However, the effects of transition metal doping on the basicity of calcined hydrotalcites (HTC-M) and their catalytic performance in the GLC synthesis remain unknown. Herein, we will show that the HTC-M samples by calcination of HT-M precursors are efficient solid base catalysts for GLC synthesis from glycerol and DMC with GLC selectivity up to 100% under moderate (100 °C) and solvent-free conditions. Their activity can be tailored by simple adjustment of the calcination temperature. The correlations between the textural, chemical structures and the basic properties of the HTC-M catalysts and the catalytic performance in the glycerol transesterification were investigated. Moreover, the optimal catalyst and reaction conditions were also determined. Our results show that the catalytic activity is proportional to the surface basic site density.

2. Experimental

2.1. Catalyst preparation

A hydrotalcite (HT) precursor with a composition of $Mg_4Al_2(OH)_{12}CO_3$ was prepared by a homogeneous precipitation method using urea hydrolysis [38]. Transition metal-doped hydrotalcite (HT-M, M = Cr^{3+}, Mn^{2+}, Fe^{3+}, Co^{2+}, Ni^{2+}, Cu^{2+}, Zn^{2+}) precursors, along with a transition-metal-free sample (HT-0), were prepared by using the calcination-reconstruction process (also known as "memory effect" of HT) [14]. Typically, a thermally decomposed HT (1.0 g calcined at 500 °C in air for 6 h) was reconstructed into the layered hydrotalcite structure along with M^{n+} cations by mixing with aqueous M^{n+} nitrate solution (0.5 mmol M^{n+}/g HT precursor) in the presence of atmospheric CO_2 (as a source of interlayer CO_3^{2-} anion) under stirring overnight at room temperature. The slurry was filtered and fully washed. The resulting solid was dried at 110 °C overnight to obtain the HT-0 and HT-M samples, which were further calcined at 500 °C in air for 6 h to yield the HTC-0 and HTC-M catalysts.

2.2. Catalyst characterization

XRD was performed on a Bruker Endeavour D4 with Cu K_α radiation (40 kV and 30 mA). SEM micrographs were taken using a FEI Quanta 200F scanning electron microscope. The BET surface areas were recorded on a Tristar 3000 automated gas adsorption system. The samples were degassed at 180 °C for 3 h prior to analysis. Magic-angle spinning (MAS) ^{27}Al NMR spectra were recorded on a Bruker DMX500 spectrometer equipped with a 4-mm MAS probe head operating at an Al NMR frequency of 130 MHz. The ^{27}Al chemical shift is referenced to a saturated $Al(NO_3)_3$ solution. In a typical experiment sample (10 mg) was packed in a 2.5 mm zirconia rotor. The MAS sample rotation speed was 25 kHz. The relaxation time was 1 s and the pulse length was 1 μs.

X-ray photoelectron spectroscopy (XPS) measurements were performed using a Thermo Scientific K-Alpha spectrometer, equipped with a monochromatic small-spot X-ray source and a 180° double focusing hemispherical analyzer with a 128-channel detector. Spectra were obtained using an aluminium anode (Al Kα = 1486.6 eV) operating at 72 W and a spot size of 400 μm. Survey scans were measured at constant pass energy of 200 eV and region scans at 50 eV. The background pressure was 2×10^{-9} mbar and during measurement 3×10^{-7} mbar Argon because of the charge compensation dual beam source. Data analysis was performed using CasaXPS software. The binding energy was corrected for surface charging by taking the C 1s peak of contaminant carbon as a reference at 284.5 eV.

Temperature programmed desorption of CO_2 (CO_2-TPD) experiments were carried out for the measurement of basicity of the catalysts. After the catalyst (50 mg) was pre-treated at 500 °C for 1 h under He stream (50 mL/min), it was cooled down to 90 °C and CO_2 (10 vol%) was introduced for adsorption at this temperature for 0.5 h. After the catalyst was swept with He for 60 min to remove the physisorbed CO_2 from catalyst surface, the temperature was increased linearly with rate of 10 °C/min in He and the signal of CO_2 (M/e = 44) was recorded by online mass spectrometry (quadrupole mass spectrometer, Balzers TPG-300). The amount of CO_2 was quantified by a calibration curve, which was established by thermal decomposition of known amounts of $NaHCO_3$.

2.3. Reaction procedure

Transesterification of dimethyl carbonate and glycerol to GLC was carried out using a 10 mL glass tube reactor with a reflux condenser. Typically, the reactor was charged with 5 mmol of glycerol, 10 wt% of catalyst (46 mg), 15 mmol of dimethyl carbonate, and 2 mmol of 1,4-butanediol (internal standard). The resulting mixture was stirred at 100 °C for 2 h then 5 mL of ethanol was added to quench the reaction. The used catalyst was separated by centrifugation, washed with ethanol and dried at 200 °C. Recovered catalyst can be reused in the next run under the same conditions. The reaction products were quantitatively analyzed by a Shimadzu QP5050 GC-MS (Stabilwax column, 30 m × 0.32 mm, d_f = 0.5 μm) using an internal standard technique.

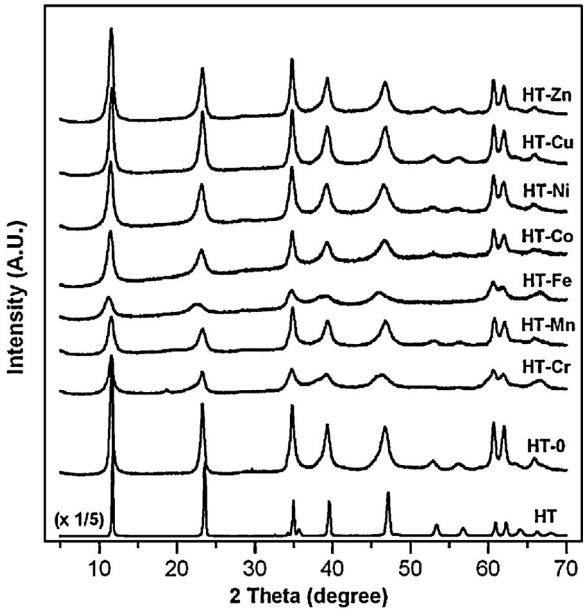

Fig. 1. XRD patterns of HT precursor and reconstructed HT-M samples.

3. Results and discussion

3.1. Catalyst preparation and characterization

To study the influence of the "calcination–reconstruction–calcination" process on the structural, morphological and textural properties of the HT-M precursors and HTC-M catalysts, various physico-chemical characterization techniques such as XRD, SEM, N_2 physisorption, ^{27}Al MAS NMR and XPS were employed. Fig. 1 shows the XRD patterns of the HT and HT-M precursors. The pattern of the HT precursor contains the characteristic peaks corresponding to a highly crystalline hydrotalcite structure [38,39]. After the calcination–reconstruction process, the well-defined hydrotalcite structure was largely retained for most HT-M samples, although the peak intensities were somewhat decreased. The structural data calculated on the basis of XRD analyses are included in Table 1. The lattice parameter c (22.72–23.57 Å, for three times of basal d(0 0 3) spacing) is consistent with the intercalation of carbonate anions. The lattice parameter a, which is about 3.05 Å for the average cation–cation distance, follows Vegard's law for solid solutions [4], and corresponds to the expected value on the basis of the Mg/Al ratio of 2. These results indicate that by adopting the "memory effect" of HT, most transition metal cations can be incorporated into the HT layers [40,41]. The XRD patterns also show that the trivalent cation-doped HT-Cr and HT-Fe samples possess less order and consist of smaller platelets than the other divalent cation-doped HT-M samples.

SEM images evidence the morphological changes after the calcination–reconstruction process (Fig. 2). The highly crystalline hexagonal plate-like morphology of the HT precursor is transformed to sunflower-like plates with many smaller flakes at the surface for all divalent cation-doped HT-M samples, indicating that the reconstruction with divalent cations mainly occurs through a surface dissolution–reprecipitation mechanism [42]. In contrast, the reconstruction with trivalent metal ions leads to more disordered morphologies, probably due to an intenser dissolution–reprecipitation process in the bulk phase. The more open structure after reconstruction is confirmed by the results of nitrogen physisorption, with much higher surface areas and pore volumes for HT-0 and HT-M samples than the HT precursor (Table 1). The higher surface areas of the HT-Cr and HT-Fe samples are consistent with the XRD and SEM results.

Solid-state ^{27}Al NMR can provide quantitative structural information on crystalline and amorphous aluminium-containing solids, because the coordination number of Al is manifested in characteristic ranges of the ^{27}Al chemical shifts [43]. Fig. 3 shows the ^{27}Al MAS NMR spectra of the HT precursor and the reconstructed HT-M samples. The signals centred at ca. 9.6 ppm, which are observed in all spectra, are attributed to six-coordinated (octahedral or AlO_6) aluminium, while a broad line centred at about 70 ppm is assigned to four-coordinated (tetrahedral or AlO_4) aluminium. The spectrum of HT precursor is characterized by a single group of AlO_6 signals. In contrast, in the spectra of HT-0 and HT-M small AlO_4 signal (<10% of the total spectral area, Table 1) occurs. Table 1 also shows the surface metal compositions of the HT precursor and the reconstructed HT-M samples. XPS data suggests a surface enrichment of Mg for divalent-metal-doped HT-M samples, but a surface enrichment of Al for HT-0, HT-Cr, and HT-Fe samples.

After calcination at 500 °C, HTC-0 and HTC-M catalysts were obtained. XRD patterns (Fig. 4) indicate that all catalysts have an MgO-like structure. However, the lattice parameter of this MgO-like structure (4.155–4.198 Å, Table 2) is smaller than that of pure MgO (4.21 Å), indicating that Al and M cations are dissolved in the lattice to form a solid solution [44]. These mixed oxides possess higher surface area and pore volume than the HT-M precursors (Table 2). XPS analysis reveals that HTC-M catalysts show higher surface M concentration but lower surface Mg^{2+} concentration than the HT-M precursors (Table 2), suggesting that the doped transition metals exist mostly at the surface of the mixed oxides. Fig. 5 presents the O 1s XP spectra for these HTC-0 and HTC-M catalysts. Three contributions are discerned at 532.9 eV, 531.5 eV and 529.7 eV. The higher binding energy (BE) peak at ~533 eV is assigned to surface adsorbed H_2O. The BE peak at 531.5 eV is

Table 1
Textural and chemical properties of HT precursor and reconstructed HT-M samples.

Sample	Lattice parameters (Å)[a]		S_{BET} (m^2/g)	Pore volume (cm^3/g)	[AlO_4] (%)[b]	Surface composition (atomic ratio)[c]	
	a	c				Mg/Al	M/Al
HT	3.045	22.726	9	0.03	0	1.81	–
HT-0	3.049	22.880	31	0.08	1.9	1.73	–
HT-Cr	3.051	22.958	103	0.42	3.0	1.71	0.14
HT-Mn	3.046	22.998	80	0.30	2.8	1.86	0.10
HT-Fe	3.050	23.568	125	0.48	2.1	1.72	0.06
HT-Co	3.049	23.158	101	0.45	9.4	1.98	0.07
HT-Ni	3.050	23.158	82	0.42	4.7	1.95	0.08
HT-Cu	3.049	22.919	83	0.34	8.6	1.91	0.08
HT-Zn	3.049	22.959	81	0.35	3.2	2.03	0.10

[a] Determined by XRD, $a = 2d$ (1 1 0), $c = 3d$ (0 0 3).
[b] Determined by 27Al MAS NMR.
[c] Evaluated by XPS.

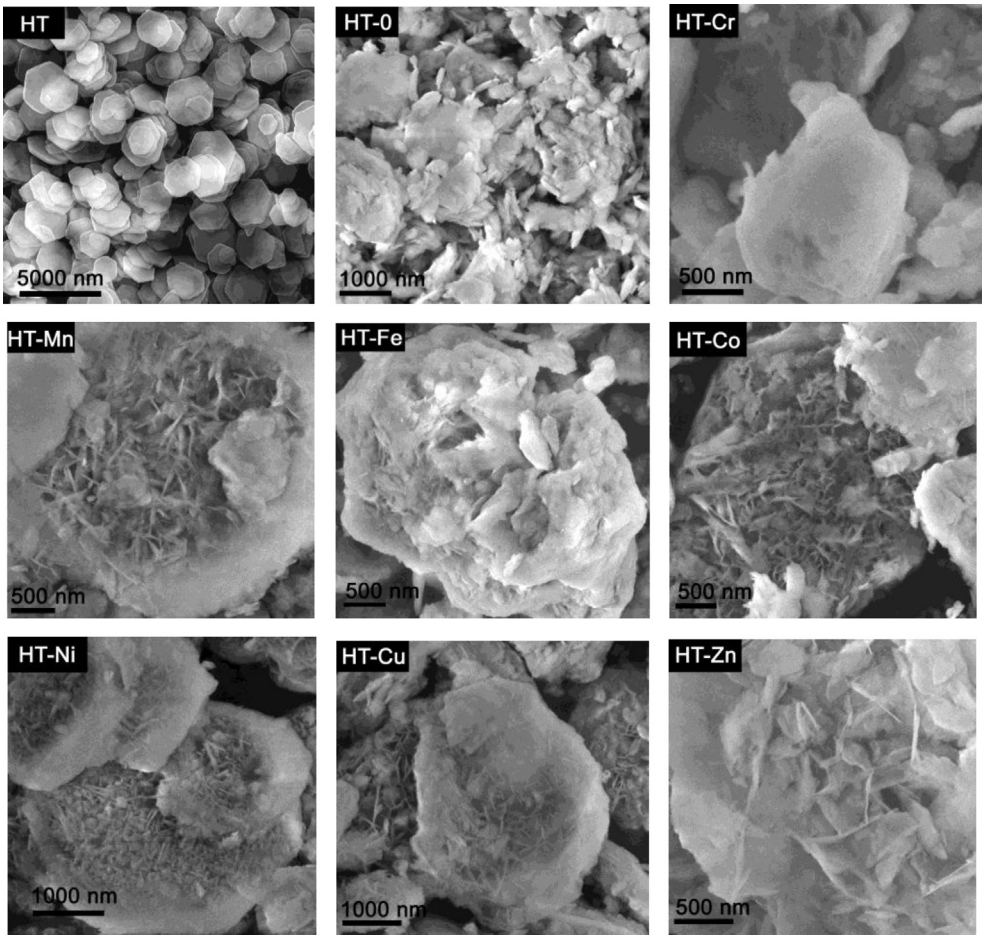

Fig. 2. SEM images of HT precursor and reconstructed HT-M samples.

attributed to the surface metal-hydroxide species. The lower BE peak at 529.7 eV is characteristic for surface O^{2-} species [45]. The significant increase in O^{2-} character is consistent with the presence of strong Lewis basic sites in the HTC-0 and HTC-M catalysts.

Fig. 6A shows a representative profile of CO_2 evolution from HT-0 during thermal decomposition. Since the quantity of CO_2 represented by the area under the decomposition curve corresponded closely to half of the Al content in the sample, it can be concluded that decomposition of the hydrotalcite is essentially complete at 500 °C for 6 h. However, calcined hydrotalcite can absorb water and CO_2 during sample exposure in air [46], as also evident from the XPS results. Therefore, the HTC-M catalysts were pre-treated under helium at 500 °C for 1 h before CO_2 adsorption. By CO_2-TPD measurements (Fig. 6B), CO_2 adsorption volumes and surface basic site densities can be evaluated (Table 3). The range of CO_2 adsorption volumes is between 0.29 mmol/g and 0.55 mmol/g, with HTC-Cr and HTC-Ni showing the lowest and the highest value, respectively. These CO_2 adsorption volumes are higher than that of previously reported MgAlNi and MgAlFe mixed oxides [36,37], mainly because of the much higher surface areas of the HTC-M catalysts. The surface basic site densities increase in the order HTC-Cr < HTC-Fe < HTC-Cu < HTC-Zn < HTC-0 < HTC-Mn < HTC-Co < HTC-Ni. The range of the density of surface basic site is between 1.2 μmol/m^2 and 2.2 μmol/m^2, in good agreement with previously reported values for calcined hydrotalcites [16,46].

Table 2
Textural and chemical properties of the HTC-M catalysts.

Sample	Lattice parameter (Å)[a]	S_{BET} (m^2/g)	Pore volume (cm^3/g)	Pore diameter (nm)[b]	Surface composition (atomic ratio)[c]	
					Mg/Al	M/Al
HTC-0	4.155	248	0.76	12.2	1.68	–
HTC-Cr	4.165	245	0.67	10.9	1.66	0.14
HTC-Mn	4.161	237	0.52	10.1	1.73	0.12
HTC-Fe	4.198	293	1.20	15.4	1.69	0.12
HTC-Co	4.173	236	0.76	13.5	1.87	0.11
HTC-Ni	4.170	248	0.85	13.7	1.86	0.12
HTC-Cu	4.166	220	0.65	11.7	1.82	0.09
HTC-Zn	4.177	222	0.68	12.2	1.93	0.12

[a] Determined by XRD.
[b] Cylindrical pore diameter (PD); PD = 4000 × pore volume/S_{BET}.
[c] Evaluated by XPS.

Table 3
Basic properties of the HTC-0 and HTC-M catalysts.[a]

Sample	CO_2 desorption peaks (area %)			Total CO_2 adsorption (mmol/g)	Basic site density (μmol/m^2)
	~165 °C	~225 °C	~325 °C		
HTC-0	31	48	21	0.44	1.8
HTC-Cr	27	48	25	0.29	1.2
HTC-Mn	28	50	22	0.45	1.9
HTC-Fe	31	43	26	0.43	1.5
HTC-Co	26	46	28	0.47	2.0
HTC-Ni	29	47	24	0.55	2.2
HTC-Cu	26	47	27	0.35	1.6
HTC-Zn	28	46	26	0.38	1.7

[a] Determined by adsorption and TPD of CO_2.

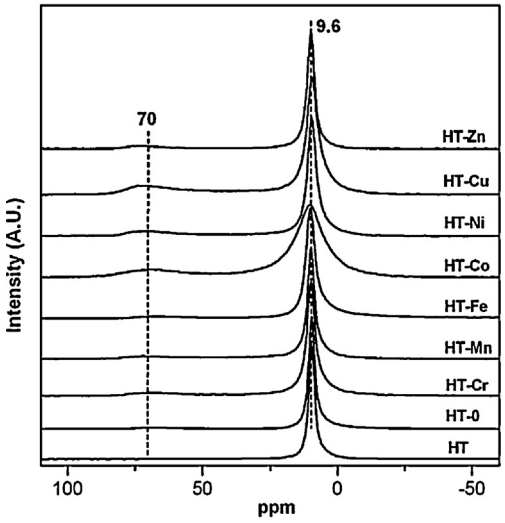

Fig. 3. ^{27}Al MAS NMR spectra of HT precursor and reconstructed HT-M samples.

The observed CO_2 desorption peaks can be used to interpret the relationship between the base strength and the calcination temperature. Higher desorption temperature and higher adsorption volume point to higher base strength. In all cases, a broad desorption band is observed between 100 °C and 500 °C (Fig. 6B), which can be deconvoluted into three main peaks at about 165 °C (weak strength), 225 °C (medium strength) and 325 °C (high strength). The medium temperature peak is more intense (43–50% of total area, Table 3). These medium-strength sites are mainly associated with Mg–O and M–O pairs [47]. The low temperature peak can be ascribed to adsorption at surface Brönsted basic site (OH^- groups). The high temperature peak is attributed to the strong Lewis basic sites of O^{2-} anions. Apparently, the base strength distribution of the HTC-M catalysts varied as a function of the doped transition metal, with Ni, Co and Mn doping showing more medium-strength basic sites (0.26 mmol/g, 0.22 mmol/g and 0.23 mmol/g, respectively) and more high-strength basic sites (0.13 mmol/g, 0.13 mmol/g and 0.10 mmol/g, respectively) than the transition-metal-free HTC-0 catalyst (0.21 mmol/g and 0.09 mmol/g for each). Consequently, the higher basicity of HTC-Ni can be attributed to the higher base strength of all three types of basic sites.

The foregoing characterization results demonstrate that the transition metal doping can be used to fine-tune the structural, textural and chemical properties of the calcined hydrotalcites. The "calcination–reconstruction–calcination" process yields HTC-M catalysts with more open structure, higher surface area, pore volume and surface transition metal concentration than the mixed oxides obtained by the direct coprecipitation–calcination approach. The nature and composition of the doped transition metal also have an influence on the surface basic site density, thus potentially affecting the catalytic performance.

3.2. Catalytic performance

3.2.1. Effect of transition metal doping

The transesterification of glycerol with dimethyl carbonate was chosen as the model reaction to evaluate the catalytic performance

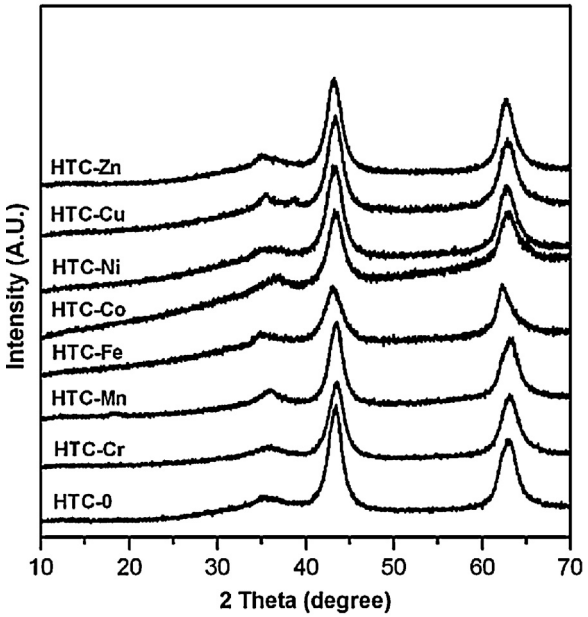

Fig. 4. XRD patterns of HTC-M catalysts.

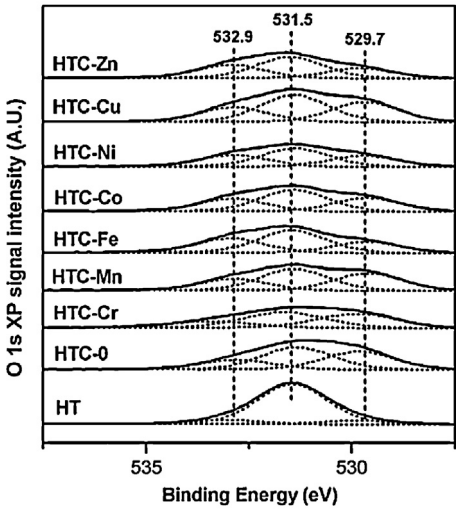

Fig. 5. O 1s XP spectra for HT precursor and HTC-M catalysts.

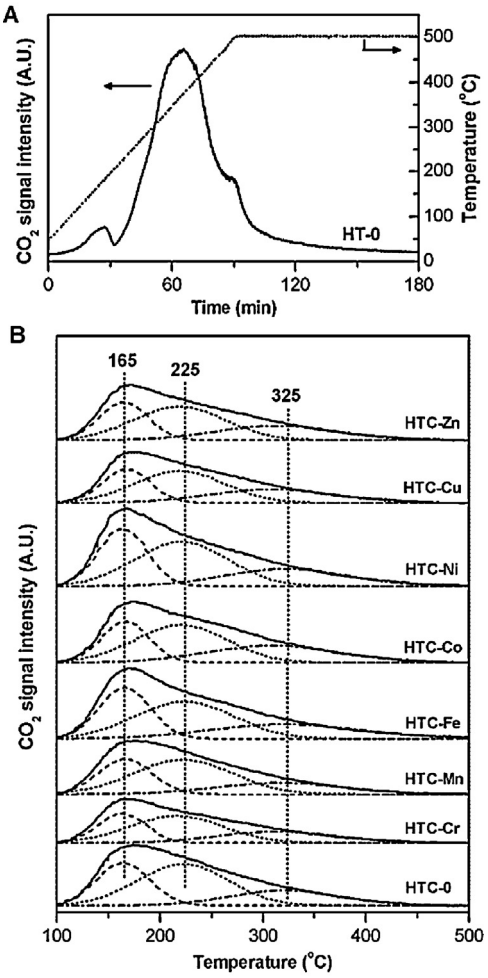

Fig. 6. (A) Release of CO_2 from HT-0 precursor during calcination in flowing He with a heating rate 5 °C/min. (B) CO_2-TPD profiles of the HTC-M catalysts.

of the various HTC-M catalysts (Scheme 1). Diethyl carbonate was not chosen as the substrate mainly due to higher reaction temperatures required for its conversion, thus resulting in lower glycerol carbonate selectivity [29–32]. The reaction was initially performed with 10 wt% of HTC-M and 3 equivalents of DMC at 100 °C under organic solvent-free conditions.

As shown in Fig. 7, the GLC yield after 2 h reaction differed significantly among the HTC-M catalysts. HTC-Cr gave the lowest yield of GLC (30%), whereas HTC-Ni achieved the highest yield (55%). The catalytic activity increased in the order HTC-Cr < HTC-Fe < HTC-Cu < HTC-Zn < HTC-0 < HTC-Mn < HTC-Co < HTC-Ni, which is in good agreement with the trend of surface basic site density. It is noteworthy that all HTC-M catalysts gave 100% GLC selectivity. The GLC yield was negligible in the absence of catalyst.

Clearly, the good correlation between the catalytic activity and the surface basic site density of HTC-M catalysts points to the importance of catalyst basicity in the transesterification reaction. It is well known that the basicity of calcined hydrotalcites depends

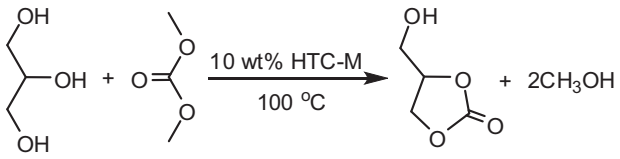

Scheme 1. Synthesis of GLC by transesterification of glycerol with DMC.

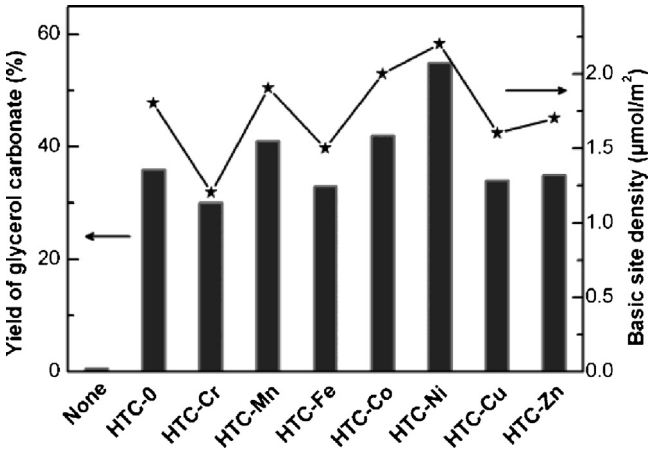

Fig. 7. Catalytic performance of HTC-M catalysts for the synthesis of glycerol carbonate. Reaction conditions: 5 mmol glycerol, 15 mmol DMC, 2 mmol 1,4-butanediol, 10 wt% of HTC-M catalyst, 100 °C, 2 h.

not only on the metal composition but also on the calcination temperature [33,45–47]. Therefore, it is possible to further improve the basicity and catalytic activity of HTC-M catalysts by varying the calcination temperature.

3.2.2. *Effect of catalyst calcination temperature*

To obtain optimum transesterification activity, various HTC-M catalysts were calcined at different temperatures (200–600 °C) before their use in the reaction. The results are presented in Table 4. Evidently, each HTC-M catalyst has its own optimum calcination temperature. HTC-Cr, HTC-Fe and HTC-Cu showed optimal activity when calcined at 400 °C. HTC-Co, HTC-Ni and HTC-Zn achieved maximum GLC yield after calcined at 500 °C. While 600 °C is the optimum calcination temperature for HTC-0 and HTC-Mn catalysts, HTC-Fe and HTC-Cr show decreased activity after being calcined at 600 °C. In all cases, GLC selectivity is 100% without any byproducts. Among various HTC-M catalysts and various calcination temperatures, HTC-Ni calcined at 500 °C exhibited the highest catalytic activity.

It can be speculated that the activity for catalysts calcined at relatively low temperature (200 °C and 300 °C) is mainly related to weak OH^- sites formed by the decomposition of surface bicarbonate species. Since calcination at 400 °C will only lead to partial decomposition, the activity is attributed to both weakly basic OH^- sites and the medium-strength Mg/M–O pair sites. After complete decomposition at higher temperature (500 °C and 600 °C), the activity can be ascribed to three kinds of basic sites, i.e. weak OH^- sites, medium Mg/M–O pair sites and strong O^{2-} sites. For the activity decrease of HTC-M catalysts at high calcination temperature (except for HTC-Mn), it is reasonable to state that the Lewis acidic nature of Al^{3+}/M^{n+} cations may suppress basicity. This speculation is supported by the fact that the surface M^{n+} concentration increased with calcination temperature, and no deactivation was observed for the transition-metal-free HTC-0 catalyst. In the case of the optimum HTC-Ni catalyst, the basicity is significantly improved, probably due to the presence of a larger amount of weak-strength OH^- sites and medium-strength Mg/Ni–O basic sites and lack of Lewis acidic defect sites of Al^{3+}/Ni^{2+} when calcined at 500 °C.

3.2.3. *Influence of reaction conditions*

The reaction conditions were further optimized for the HTC-Ni catalyst. Fig. 8A shows the effect of reaction temperature. The GLC yield was increased with reaction temperature up to 100 °C and, thereafter, there was a significant decrease in yield. The HTC-Ni catalyst showed maximum activity at a reaction temperature

Table 4
Effect of catalyst calcination temperature on glycerol transesterification activity.[a]

Catalyst	Yield of GLC (%)				
	200 °C	300 °C	400 °C	500 °C	600 °C
HTC-0	36	41	31	36	42
HTC-Cr	21	41	42	30	3
HTC-Mn	23	19	26	41	48
HTC-Fe	30	23	39	33	0
HTC-Co	9	32	33	42	31
HTC-Ni	27	28	40	55	22
HTC-Cu	25	18	44	34	12
HTC-Zn	34	33	19	35	22

[a] Reaction conditions: 5 mmol glycerol, 15 mmol DMC, 2 mmol 1,4-butanediol (internal standard), and 10 wt% of HTC-M, 100 °C, 2 h.

of 100 °C. The decreased GLC yield (with 100% selectivity) at high temperature suggests that side-reactions (dehydrogenation and condensation) by the byproduct methanol may occur on the basic sites, although these by-products were not observed in GC–MS analysis because of the strong signal overlap by that of the solvent. Fig. 8B presents the influence of the catalyst amount on transesterification reaction. Surprisingly, the GLC yield was not increased when the amount of catalyst was increased. Compared to 10 wt% of catalyst, the activity was even lower when 20 wt% of catalyst was used. When 15 wt% of catalyst was used the GLC yield was similar. This is mainly due to the increased resistance of mass transfer in the solid catalyst–glycerol–DMC triphase system, because catalyst aggregation was clearly observed when catalyst amount increased to more than 10 wt%.

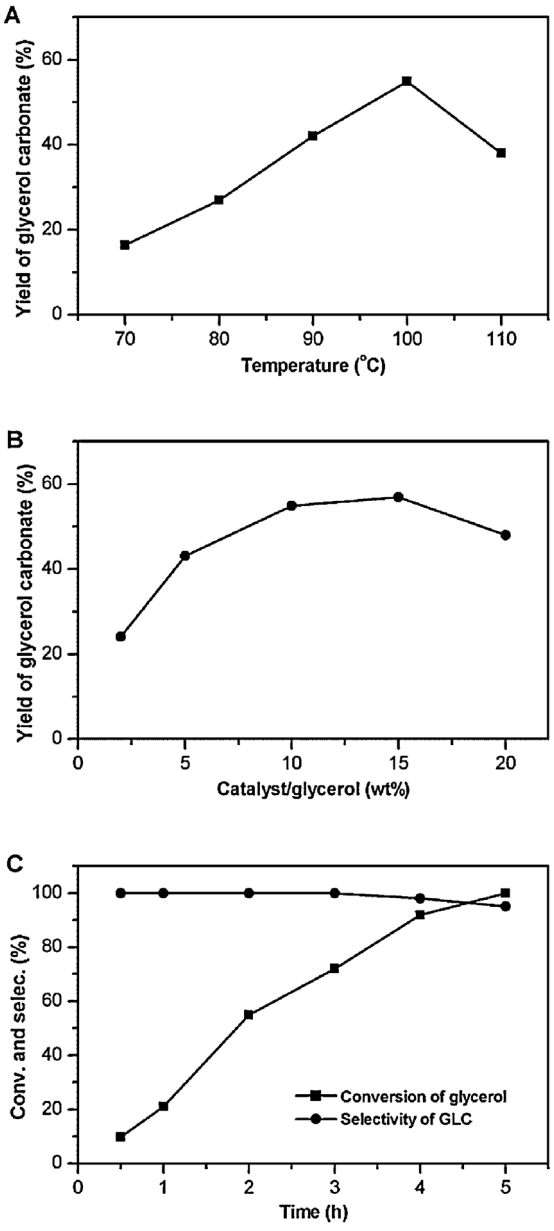

Fig. 8. Effect of reaction temperature (A), catalyst amount (B) and reaction time (C) on catalytic performance of HTC-Ni catalyst. Typical reaction conditions: 5 mmol glycerol, 15 mmol DMC, 2 mmol 1,4-butanediol, 10 wt% of HTC-Ni, 100 °C, 2 h.

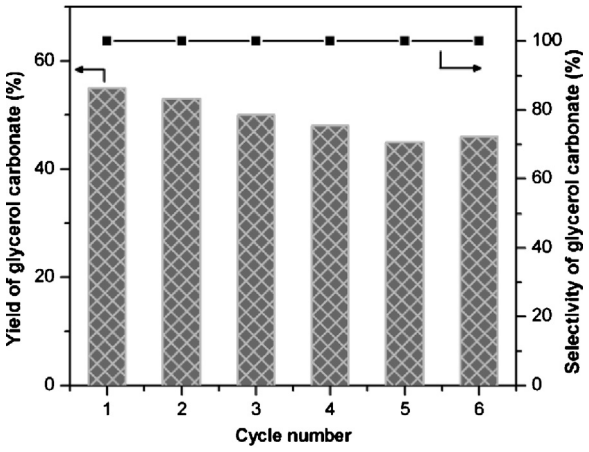

Fig. 9. Reusability of HTC-Ni catalyst. Reaction conditions: 5 mmol glycerol, 15 mmol DMC, 2 mmol 1,4-butanediol, 100 °C, 2 h; for the first cycle, 10 wt% of HTC-Ni catalyst was added.

The optimum reaction temperature and catalyst amount were determined to be 100 °C and 10 wt%, respectively. Under these conditions, the effect of reaction time was also investigated and the results are shown in Fig. 8C. Clearly, the transesterification reaction has no induction period. The reaction achieved 100% conversion of glycerol after 5 h but with a slight decrease in GLC selectivity (95%). Glycerol dicarbonate was identified to be the only by-product of glycerol, which is generally reported as the main by-product for GLC synthesis by transesterification of glycerol with alkyl carbonates and the selectivity can reach up to 30–80% by other calcined or rehydrated hydrotalcite catalysts [29–32]. The decrease in GLC selectivity is indicative of some deactivation of the HTC-Ni catalyst and could be attributed to a strong adsorption of side products (mainly derived from methanol) on the basic sites during the reaction.

3.2.4. Stability of HTC-Ni catalyst

In order to obtain the information on the stability of HTC-Ni catalyst, the spent catalyst was recycled in the glycerol transesterification reaction and the results are presented in Fig. 9. The solid catalyst could be readily separated from the reaction mixture by

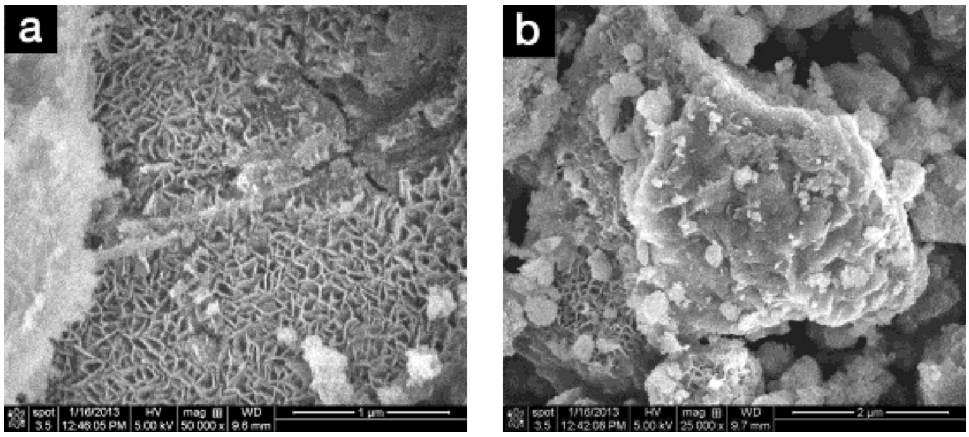

Fig. 10. SEM images of the fresh (a) and fifth recycled (b) HTC-Ni catalyst.

centrifugation and used in next cycle after washing and drying. To our delight, HTC-Ni could be recycled and reused at least five times without significant loss of activity and selectivity, and the GLC selectivity retained 100% even after the repetitive use. The gradual conversion decrease from 55% to 45% can be partially attributed to the weight loss during catalyst recovery, because a loss of catalyst of about 8% was observed after the fifth reuse. Subsequently, the fifth recycled catalyst was tested by SEM, XRD and XPS. SEM shows that the sheet-like morphology was unchanged (Fig. 10), although many smaller sized particles are present on the recycled catalyst, which can be due to the collision and attrition induced by the stirrer. XRD results confirm retention of the original MgO-like structure (Fig. 11A). XPS evidences a different surface metal composition for the recycled catalyst with Mg/Ni/Al = 2.17:0.12:1.00. Compared to the fresh catalyst, a significant increase in surface Mg concentration was observed, indicating that more Mg^{2+} in the bulk phase gradually transferred to the surface. Fig. 11B shows the O 1s XP spectra for the fresh and fifth recycled HTC-Ni catalyst. The decrease in O^{2-} character (529.7 eV) for the reused catalyst supports the speculation that side products may adsorb on the strong basic sites during the reaction. From the structural information of the recycled HTC-Ni catalyst, the reconstruction of the layered HT structure by the "memory effect" can be excluded. This is mainly due to the anhydrous conditions applied during reaction and catalyst recovery processes. Significantly, the optimum HTC-Ni catalyst showed higher stability than previously reported rehydrated HT catalysts in the transesterification of glycerol to GLC [29,30].

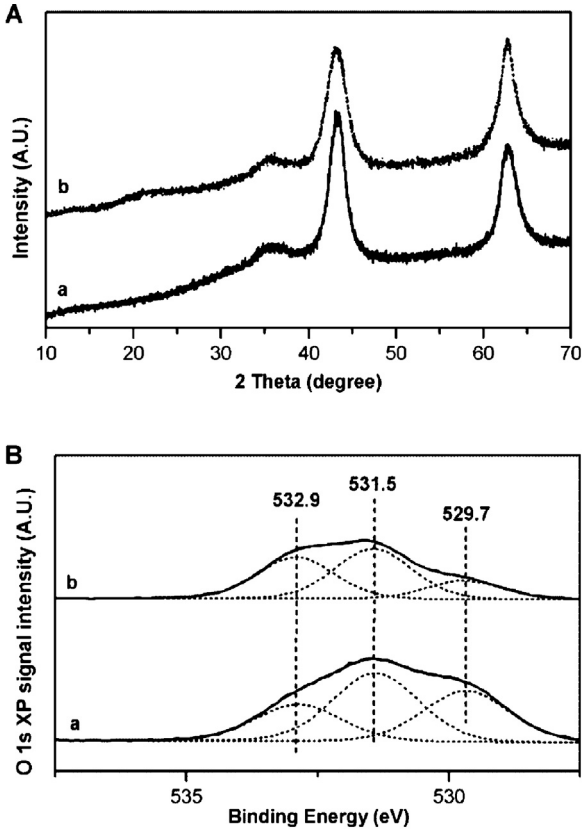

Fig. 11. XRD patterns (A) and XP spectra (B) of the fresh (a) and fifth recycled (b) HTC-Ni catalyst.

Table 5
Comparison of the catalytic activity of HTC-Ni with other reference catalysts for the synthesis of glycerol carbonate.[a]

Catalyst	Time (h)	GLC yield (%)	GLC selectivity (%)
HTC-Ni	2	55	100
HT-Ni	2	21	100
HT	2	5	100
MgO[b]	2	50	100
CaO[c]	1	79	81
NaOH[d]	1	70	70

[a] Reaction conditions: 5 mmol glycerol, 15 mmol DMC, 2 mmol 1,4-butanediol, and 10 wt% of catalyst, 100 °C.
[b] Calcined at 600 °C.
[c] Calcined at 900 °C.
[d] 2 wt% of catalyst was used.

3.2.5. Activity comparison of the HTC-Ni catalyst with other reference catalysts

Since most previous studies use quite different reaction conditions, it is difficult to directly compare the activity of our HTC-Ni catalyst with previously reported base catalysts. Therefore, we prepared and compared several representative reference catalysts under our reaction conditions and the results are shown in Table 5. Evidently, the HT-Ni precursor showed much lower activity than HTC-Ni catalyst, mainly due to the presence of only weak-strength basic sites in the uncalcined sample. Furthermore, HT precursor is about ten times less active than HTC-Ni catalyst, which is ascribed to both the weak basicity and the very low surface area of HT precursor. HTC-Ni outperforms MgO under identical conditions, demonstrating the promotional effect of Ni^{2+} doping on catalyst basicity and activity. CaO and NaOH exhibited much higher activity but with significantly lower GLC selectivity, in agreement with previously reported results [48,49]. Moreover, CaO cannot be reused unless regenerated at high temperature (900 °C) [48]. Based on the

above results, we can conclude that the HTC-Ni is a stable and practical catalyst for glycerol carbonate synthesis by glycerol transesterification with dimethyl carbonate.

4. Conclusions

In summary, we have described a facile "calcination–reconstruction–calciantion" procedure for the doping of transition metal cations into hydrotalcite precursors to afford efficient heterogeneous base catalysts. Using the "memory effect" of hydrotalcite, the synthesized HTC-M catalysts can possess more open structure and higher basicity. The basicity can be fine-tuned by simple adjustment of the final calcination temperature. The catalytic performance of the HTC-M catalysts in organic solvent-free transesterification of glycerol with dimethyl carbonate strongly depends on the type of transition metal, the surface basicity and the reaction conditions. A good correlation between catalytic activity and surface basic site density of the HTC-M catalysts has been established. HTC-Ni catalyst calcined at 500 °C shows maximum activity, which has been attributed to the enhancing effect of Ni^{2+} doping on the strength of all three types of basic sites. Insight in these findings might make it possible to design more efficient solid base catalysts for various base-catalyzed reactions.

Acknowledgment

This research was financially supported by Programme Strategic scientific Alliances between the Netherlands and China (Grant No. 2008DFB5-130).

References

[1] H. Hattori, Chemical Reviews 95 (1995) 537.
[2] G. Busca, Industrial and Engineering Chemistry Research 48 (2009) 6486.
[3] G. Busca, Chemical Reviews 110 (2010) 2217.
[4] F. Cavani, F. Trifiró, A. Vaccari, Catalysis Today 11 (1991) 173.
[5] D. Tichit, B. Coq, Catalysis Technology 7 (2003) 206.
[6] D.P. Debecker, E.M. Gaigneaux, G. Busca, Chemistry – A European Journal 15 (2009) 3920.
[7] J. He, M. Wei, B. Li, Y. Kang, D.G. Evans, X. Duan, Structure and Bonding 119 (2006) 89.
[8] B.F. Sels, D.E. de Vos, P.A. Jacobs, Catalysis Reviews Science and Engineering 43 (2001) 443.
[9] F. Figueras, Topics in Catalysis 29 (2004) 189.
[10] D. Tichit, C. Gérardin, R. Durand, B. Coq, Topics in Catalysis 39 (2006) 89.
[11] Z.P. Xu, J. Zhang, M.O. Adebajo, H. Zhang, C. Zhou, Applied Clay Science 53 (2011) 139.
[12] P. Liu, H. Wang, Z. Feng, P. Ying, C. Li, Journal of Catalysis 256 (2008) 345.
[13] P. Liu, C. Wang, C. Li, Journal of Catalysis 262 (2009) 159.
[14] P. Liu, Y. Guan, R.A. van Santen, C. Li, E.J.M. Hensen, Chemical Communications 47 (2011) 11540.
[15] P. Liu, C. Li, E.J.M. Hensen, Chemistry – A European Journal 18 (2012) 12122.
[16] A.L. Mckenzie, C.T. Fishel, R.J. Davis, Journal of Catalysis 138 (1992) 547.
[17] A. Corma, V. Fornés, F. Rey, Journal of Catalysis 148 (1994) 205.
[18] J.C.A.A. Roelofs, D.J. Lensveld, A.J. van Dillen, K.P. de Jong, Journal of Catalysis 203 (2001) 184.
[19] F. Winter, X. Xia, B.P.C. Hereijgers, J.H. Bitter, A.J. van Dillen, M. Muhler, K.P. de Jong, Journal of Physical Chemistry B 110 (2006) 9211.
[20] C.-H. Zhou, J.N. Beltramini, Y.-X. Fan, G.Q. Lu, Chemical Society Reviews 37 (2008) 527.
[21] M. Pagliaro, R. Ciriminna, H. Kimura, M. Rossi, C.D. Pina, Angewandte Chemie International Edition 46 (2007) 4434.
[22] A. Behr, J. Eilting, K. Irawadi, J. Leschinski, F. Lindner, Green Chemistry 10 (2008) 13.
[23] J.R. Ochoa-Gómez, O. Gómez-Jiménez-Aberasturi, C. Ramírez-López, M. Belsué, Organic Process Research and Development 16 (2012) 389.
[24] M.O. Sonnati, S. Amigoni, E.P.T. de Givenchy, T. Darmanin, O. Choulet, F. Guittard, Green Chemistry 15 (2013) 283.
[25] M.J. Climent, A. Corma, P.D. Frutos, S. Iborra, M. Noy, A. Velty, P. Concepción, Journal of Catalysis 269 (2010) 140.
[26] S.-I. Fujita, Y. Yamanishi, M. Arai, Journal of Catalysis 297 (2013) 137.
[27] A. Takagaki, K. Iwatani, S. Nishimura, K. Ebitani, Green Chemistry 12 (2010) 578.
[28] A. Kumar, K. Iwatani, S. Nishimura, A. Takagaki, K. Ebitani, Catalysis Today 185 (2012) 241.
[29] M.G. Álvarez, A.M. Segarra, S. Contreras, J.E. Sueiras, F. Medina, F. Figueras, Chemical Engineering Journal 161 (2010) 340.
[30] M.G. Álvarez, R.J. Chimentao, F. Figueras, F. Medina, Applied Clay Science 58 (2012) 16.
[31] M.G. Álvarez, M. Pliskova, A.M. Segarra, F. Medina, F. Figueras, Applied Catalysis B 113/114 (2012) 212.
[32] M.G. Álvarez, A.M. Frey, J.H. Bitter, A.M. Segarra, K.P. de Jong, F. Medina, Applied Catalysis B 134/135 (2013) 231.
[33] M. Malyaadri, K. Jagadeeswaraiah, P.S.S. Prasad, N. Lingaiah, Applied Catalysis A 401 (2011) 153.
[34] S. Kannan, Catalysis Surveys From Asia 10 (2006) 117.
[35] G.S. Macala, A.W. Robertson, C.L. Johnson, Z.B. Day, R.S. Lewis, M.G. White, A.V. Iretskii, P.C. Ford, Catalysis Letters 122 (2008) 205.
[36] Y.-B. Wang, J.-M. Jehng, Chemical Engineering Journal 175 (2011) 548.
[37] S.-H. Wang, Y.-B. Wang, Y.-M. Dai, J.-M. Jehng, Applied Catalysis A 439/440 (2012) 135.
[38] M. Ogawa, H. Kaiho, Langmuir 18 (2002) 4240.
[39] M. Adachi-Pagano, C. Forano, J.-P. Besse, Journal of Materials Chemistry 13 (2003) 1988.
[40] K. Takehira, T. Shishido, Catalysis Surveys From Asia 11 (2007) 1.
[41] S.K. Jana, Y. Kubota, T. Tatsumi, Journal of Catalysis 247 (2007) 214.
[42] M. Rajamathi, G.D. Nataraja, S. Ananthamurthy, P.V. Kamath, Journal of Materials Chemistry 10 (2000) 2754.
[43] A. Vyalikh, F.R. Costa, U. Wangenknecht, G. Heinrich, D. Massiot, U. Scheler, Journal of Physical Chemistry C 113 (2009) 21308.
[44] F. Millange, R.I. Walton, D. O'Hare, Journal of Materials Chemistry 10 (2000) 1713.
[45] D.G. Cantrell, L.J. Gillie, A.F. Lee, K. Wilson, Applied Catalysis A 287 (2005) 183.
[46] P. Liu, M. Derchi, E.J.M. Hensen, Applied Catalysis A 2013, http://dx.doi.org/10.1016/j.apcata.2013.07.020
[47] J.I.D. Cosimo, V.K. Díez, M. Xu, E. Iglesia, C.R. Apesteguía, Journal of Catalysis 178 (1998) 499.
[48] J.R. Ochoa-Gómez, O. Gómez-Jiménez-Aberasturi, B. Maestro-Madurga, A. Pesquera-Rodríguez, C. Ramírez-López, L. Lorenzo-Ibarreta, J. Torrecilla-Soria, M.C. Villarán-Velasco, Applied Catalysis A 366 (2009) 315.
[49] R. Bai, Y. Wang, S. Wang, F. Mei, T. Li, G. Li, Fuel Processing Technology 106 (2013) 209.